International Journal of Automotive Technology, Vol. 8, No. 6, pp. 723–730 (2007)

1229-9138/2007/037-07

MEASUREMENT AND CHARACTERIZATION OF FRICTION IN AUTOMOTIVE DRIVESHAFT JOINTS

C.-H. LEE*

Department of Mechanical Engineering, Inha University, Incheon 402-751, Korea

(Received 25 January 2007; Revised 6 September 2007)

ABSTRACT–The typical design of automotive driveshafts generally utilizes Constant Velocity (CV) joints as a solution to NVH. CV joints are an integral part of vehicles and significantly affect steering, suspension, and vehicle vibration comfort levels. Thus, CV joints have been favored over universal joints due to the constant velocity torque transfer and plunging capability. Although CV joints are common in vehicle applications, current research works on modeling CV joint friction and assumes constant empirical friction coefficient values. However, such models are long known to be inaccurate, especially under dynamic conditions, which is the case for CV joints. In this paper, an instrumented advanced CV joint friction apparatus was developed to measure the internal friction behavior of CV joints using actual tripod-type joint assemblies. The setup is capable of measuring key performance of friction under different realistic operating conditions of oscillatory speeds, torque and joint installation angles. The apparatus incorporates a custom-installed tri-axial force sensor inside of the joint to measure the internal CV joint forces (including friction). Using the designed test setup, the intrinsic interfacial parameters of CV joints were investigated in order to understand their contact and friction mechanisms. The results provide a better understanding of CV joint friction characteristics in developing improved automotive driveshafts.

KEY WORDS : Automotive driveshaft; Constant Velocity joints; Friction test; Automotive tribology

1. INTRODUCTION

It is well known that the Constant Velocity (CV) joint is the standard design for the automotive driveshaft joint due to its superior performance in eliminating uneven rotating torque compared to universal joints (Hooke's and Cardan joints are also used interchangeably). This is achieved through their self-centering properties (Schmelz *et al.*, 1992; Wagner, 1979). Typically, each driveshaft is comprised of two types of CV joints, fixed and plunging types connected by a solid shaft. Current research is emphasized on a class of CV joints called tripod joints, which have been favored especially for automatic transmission vehicles. This is due to their noise and vibration advantages offering lower plunging resistance, compared to ball-type joints.

Although CV joints are common in vehicles, there are certain aspects of their internal friction dynamic that is not fully understood or modeled. These effects are not generally predictable and repeatable, thus causing uncertainty in performance reliability predictions.

A typical vehicle problem associated with CV joints is the so-called "take off shudder," which generally occurs when the vehicle moves (starts) abruptly. This problem is primarily related to the internal friction in the CV joint, which consequently generates an axial force know as Generated Axial Force (GAF). The other problem accounting for vehicle vibration is "idle boom". As the plunging joint is directly connected to the gearbox, whereby the engine excites, there is a transfer of vibration to driveshafts, even when the vehicle is stationary.

To avoid such potential problems, extensive testing with all new vehicle models is usually undertaken leading to longer development periods. Better understanding of the non-linear dynamic interfacial friction behavior of CV joints can provide powerful design tools and lead to the development of basic CV joint friction models. Because of the importance of CV joints as well as their complexity, a specialized CV joint apparatus has been presented in the literature to measure different aspects of CV joint behavior. For example, Philpott *et al.* (1996) developed a tester and implemented a two-phase surface fitting regression algorithm to quantify the race track wear in CV joints. Bierman (1999) designed an apparatus to accurately measure the efficiency of CV joints by recording power and heat losses. Kernizan *et al.* (2002) developed a tester to assess the performance of grease by measuring the temperature increase in CV joints. Jia *et al.*

*Corresponding author. e-mail: chulhee@inha.ac.kr

(2002) investigated the dynamic performance of tripod-type CV joints, and designed an experimental tester to measure the effect of the clearance on their dynamic response. Lastly, Kochersberger (2002) patented an apparatus to detect defects in CV joints by measuring irregular vibration patterns. However, despite these advances in measuring CV joint parameters, none of these works directly measures internal CV joint friction.

In this paper, the author presents an advanced well-instrumented CV joint apparatus to experimentally investigate the internal friction in CV joints. The intrinsic interfacial parameters, such as the torque, articulation angle, plunging velocity and rotational phase of CV joints, are investigated in order to understand their contact and friction mechanisms. Such measurements will provide a better understanding of CV joint friction characteristics that can be used in developing improved CV joints

2. DEVELOPMENT OF APPARATUS

2.1. CV Joint Friction Apparatus

A dedicated and instrumented CV joint apparatus was designed and constructed to conduct controlled realistic experiments to measure friction of actual (full scale) CV joints. This tester enables measurements of key performance parameters, such as internal friction between ball and housing groove under realistic operating conditions. These experiments established a set of critical parameters and provided useful information about CV joint internal friction that was not previously available. An overall schematic of the apparatus is shown in Figure 1, and the main capabilities of the apparatus are: (i) statically control and vary the CV joint installation (also known as articulation) angle; (ii) control and vary the input torque; (iii) control and vary the linear stroke motion; and (iv) test the actual tripod CV joints.

In the CV joint friction apparatus, the sliding motion mechanism provides a plunging motion (stroke) using a linear actuator and servo-motor control drive. The linear plunging motion was controlled by a linear brushless servo controller using programmed PLC sequential codes. Using the quadrature encoder resolution of the linear actuator, the linear displacement and velocity were precisely controlled. A fixture was also designed to directly attach the ball joint part of the CV joint assembly to the linear actuator. This fixture can adjust the height of one of the ends of the CV joint, thus being able to change the CV joint articulation angle, which is a major factor affecting the plunging joint friction during the experiments to simulate the articulation angle and plunging motions in the CV joint due to wheel bouncing as well as steering motion and engine movement. The apparatus was designed to supply a maximum articulation angle of 15°, a plunging force of 100 N and a maximum oscillation frequency of 25 Hz. The static torque is applied manually with a hand crank and worm gearbox mechanism to simulate the torque loading under the abrupt start of actual vehicles. Figure 2 shows the constructed static torque generating mechanisms with the part name indicated. The design is such that it can generate a maximum static torque of 1000 Nm. This mechanism was also used to attach the actual tripod joint to the static torque generator. This part utilizes a thrust bearing as the sliding resistance and also generates a thrust force at the bearing. The applied torque and generated thrust force are measured directly using a force/torque strain gage transducer attached between the CV joint and the torque mechanism. As the linear actuator initiates the CV joint movement, two displacement measurements are monitored using (a) the encoder that is inside the linear actuator and (b) an external LVDT displacement sensor that is in

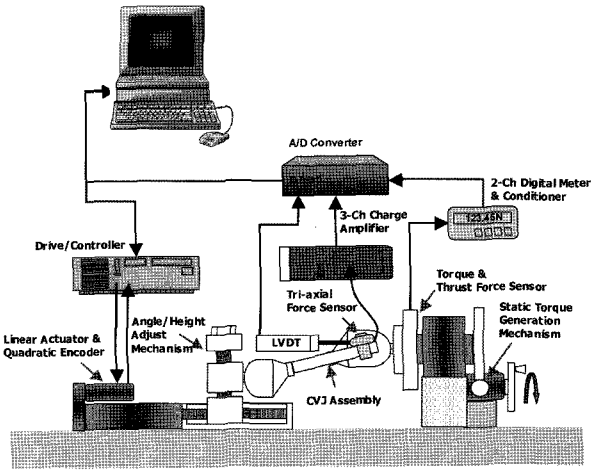

Figure 1. Schematic diagram of the CV joint friction apparatus.

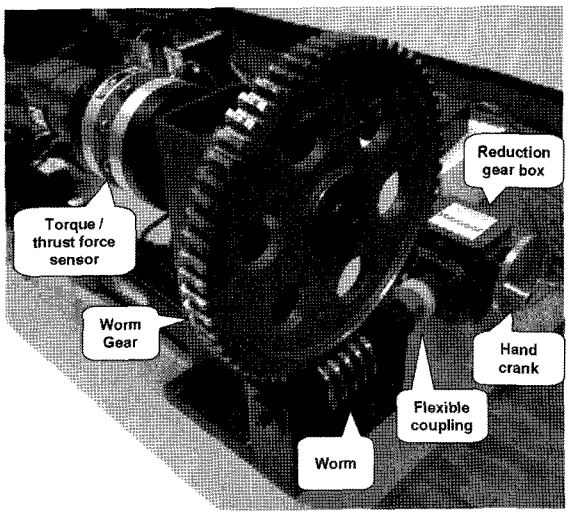

Figure 2. Photograph of torque generating mechanism.

contact with the spider inside the CV joint. Thus, the encoder measures the input displacement to the CV joint and the LVDT measures the net resultant movement of the CV joint during experiments. In this work, both the displacement measurements were found to be coincident, implying that there was no significant backlash in the system.

A Labview program was developed to control the overall experimental setup directly from a PC after completion of designing and building the CV joint apparatus. Specifically, Labview was used as a digital oscilloscope, triggering mechanism, controlling the linear motion and also recording the experimental output data. Such master control program provides accurate triggering and synchronizing of the apparatus components while concurrently capturing and digitally recording all measurements. The linear actuator, which generates the force to linearly move the CV joint, is controlled by the computer via a drive/controller. To precisely measure the torque applied to the CV joint with the static torque generator, a two axis strain-gage force/torque sensor was installed and the outputs were displayed on digital meters and also fed to the PC for digital recording. The thrust force output that is typically measured in the conventional experiments represents the combined CV joint frictional and other internal forces. The internal tri-axial friction forces were measured directly using the embedded tri-axial force transducer, and the signal output was fed to the computer via signal conditioners and A/D converters.

2.2. Internal Friction Measurement

A unique feature of the apparatus utilized in this paper is that the actual CV joint is retrofitted with a three axis piezoelectric force transducer for *in situ* measurement of internal CV joint forces including friction. This is accomplished by precisely cutting out one of the trunnions, and then milling a hole where the force transducer is inserted with a very small tolerance (Figure 3(b)).

Subsequently, the trunnion was reassembled using the tri-axial force transducer's preload bolt as shown in Figure 3(a). Then, the tri-axial forces were calibrated using the manufacturer's suggested calibration procedures, and confirmed that the manufacturer's specifications were confirmed to be correct using dead weights. A possible concern in this tri-axial force transducer design was the cross-talk between each orthogonal force axis, which was measured and in all cases found to be less than 2%, which is less than the manufacturer's specification.

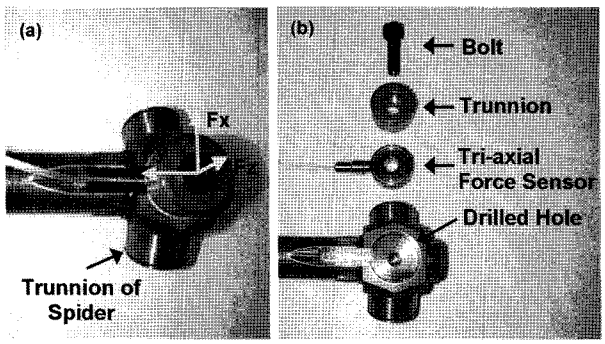

Figure 3. Installation of tri-axial force transducer: (a) assembled; (b) disassembled.

3. MEASUREMENT OF FRICTION

3.1. Test Procedure

In-production and fully assembled tripod type CV joints were procured and installed on the apparatus shown in Figure 1. The ball joint side of the CV joint is clamped to the apparatus using a machined spline, whereas the tripod joint side is clamped using a tight-fit interference with secure clamping. After secure clamping of the CV joint on the apparatus, its position was articulated and preset to a specified articulation angle by adjusting the height mechanism and measuring the articulation angle using a precise digital level gage.

As the tests were performed under loaded conditions, a static torque was applied to the CV joint by cranking the worm gear mechanism. The preset static torque values were measured on the digital display of the torque transducer with typical static torque values. After setting the CV joint assembly at the designated articulation angle and the static torque, experiments were performed by plunging the CV joint two full cycles of +15 mm and −15 mm from the joint center position with a typical velocity of 2 mm/sec. This is a typical travel distance in actual automotive CV joints and simulates the wheel bouncing and steering motion in vehicle. All CV joint friction experiments were performed under grease lubricated conditions with the typical CV joint used in a North American vehicle. Experiments were repeated at two different articulation angles, these being 0° representing idealistic conditions with minimal internal friction and GAF, and 15° representing aggressive conditions with significant CV joint friction and GAF. Typical experi-

Table 1. Typical experimental conditions.

Temperature	22.5°C
Humidity	40-50% RH
Articulation angle (β)	0-15°
Linear stroke	± 15 mm (2 cycles)
Stroke velocity	2 mm/sec
Applied torque	0-160 Nm static
Grease	Polyurea type, Solid EP additives

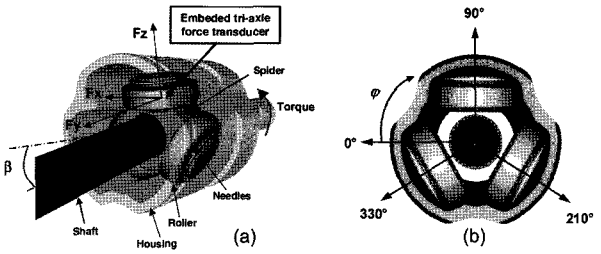

Figure 4. Coordinates and definitions in tripod CV joint contact: (a) tri-axial force coordinates and terminology; (b) definition of rotational phase angle.

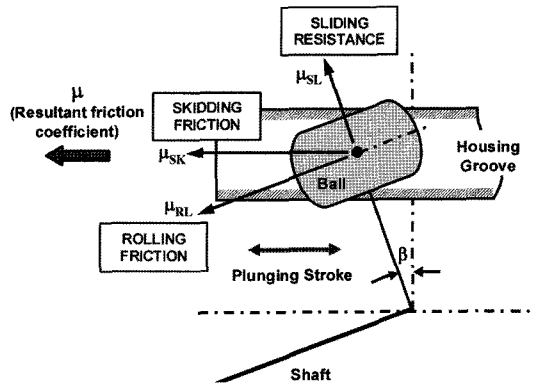

Figure 5. Internal friction forces and friction coefficient at a trunnion inside tripod CV joint.

mental conditions used in this study are summarized in Table 1.

Terminologies in typical tripod CV joint components are shown in Figure 4(a). The directions of the three force components measured with the tri-axial force sensor installed inside the CV joint are also depicted in Figure 4(a). The force component Fx represents the normal force P and is directly related to the applied torque. The force components Fy and Fz represent the axial and vertical friction forces respectively, which are the source of the total combined friction force Q. Figure 4(b) defines the CV joint rotational phase angle φ from the housing end view.

3.2. Friction Coefficient

The major internal friction components and friction coefficients inside the tripod CV joint are depicted schematically in Figure. 5. Skidding friction, which is represented by μ_{SK}, is generated along the housing groove, and is believed to be the dominant friction that causes GAF. The rolling friction, represented by rolling friction coefficient μ_{RL}, is the pure rolling friction term in roller. This value could be estimated using the slip to roll ratio during the plunging motion. Finally, the sliding resistance μ_{SL} is the overall friction resistance between the needles and the roller and also between the needles and spider during the up and down motion of the roller. Thus, combining these friction force components, the resultant friction coefficient m in terms of the housing coordinate can be obtained, and is this value that will then be used to estimate the GAF.

As shown in Figure 5, one can calculate the resultant friction coefficient μ at the CV joint from the measurement of internal friction forces by using the following simple equation:

$$\mu=\frac{F_y \cos\beta+F_z \sin\beta}{F_x} \tag{1}$$

Where β is the CV joint articulation angle, as also depicted in Figure 5. However, this equation is only valid when the trunnion with the tri-axial force sensor is in the top position, which is defined as a 90° of the rotational phase angle j in Figure 4(b).

In order to calculate the internal friction coefficient that is present under all CV joint conditions, one needs to find a universal equation to cover all articulation and rotational phase angles. This is accomplished by introducing a coordinate transformation matrix based on Euler angles representing articulation angle β, and rotational phase angle φ. By using the defined coordinates of the tri-axial forces shown in Figure 4(a), the individual transformation matrix for each rotation and articulation in sequence can be obtained. By multiplying each individual transformation matrix, the following equation relating the measured internal forces to the global forces in accordance with the housing coordinate is given by:

$$\begin{bmatrix} Fx''' \\ Fy''' \\ Fz''' \end{bmatrix} = \begin{bmatrix} \cos^2(\varphi-90°)+\cos\beta\sin^2(\varphi-90°) & -\sin(\varphi-90°)\sin\beta & \cos(\varphi-90°)\sin(\varphi-90°)[-1+\cos\beta] \\ \sin(\varphi-90°)\sin\beta & \cos\beta & \cos(\varphi-90°)\sin\beta \\ \cos(\varphi-90°)\sin(\varphi-90°)[-1+\cos\beta] & -\cos(\varphi-90°)\sin\beta & \cos^2(\varphi-90°)\cos\beta+\sin^2(\varphi-90°) \end{bmatrix} \begin{bmatrix} Fx \\ Fy \\ Fz \end{bmatrix} \tag{2}$$

Thus, one can calculate the net friction coefficient along the housing groove at any rotational and articulation position with the following equation:

$$\mu=\frac{Fy'''}{Fx'''} \tag{3}$$

4. EXPERIMENTAL RESULTS

4.1. Typical Test Results

Typical experiments captured over two complete cycles (60 seconds) under 160 Nm static torque are depicted in Figure 8, at two different articulation angles of 0° and 15°. As shown in Figure 6(a), the experiments begins with the CV joint spider being in the center position of the housing, then moving inwards in the housing for 15 mm, and then moving all the way towards the outward position of the housing, passing through the center position and then moves to the center position. The exact

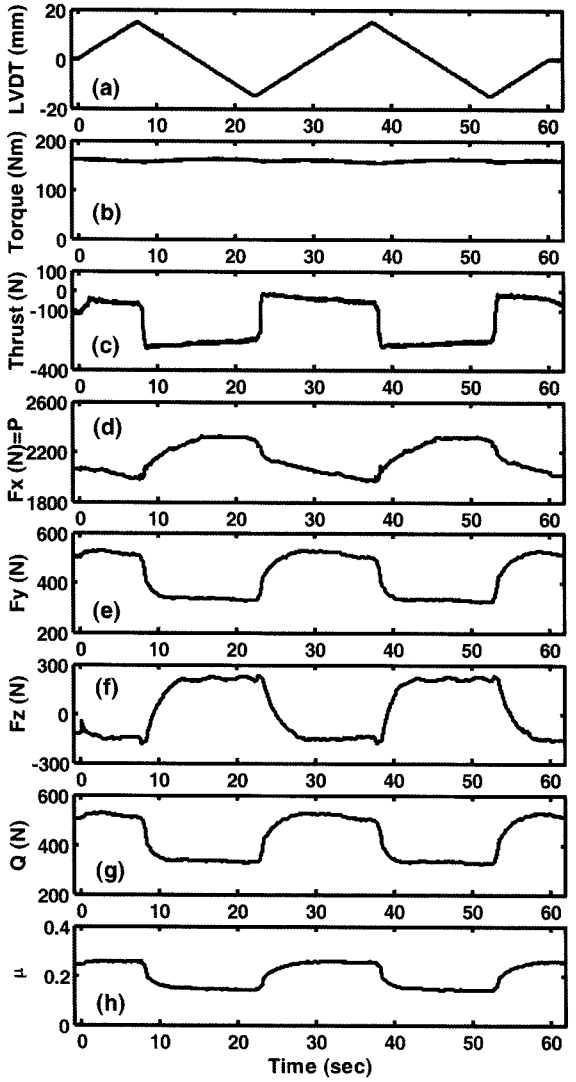

Figure 6. Measurement data during CV joint stroke motion at the extreme articulation angles.

same cycle is repeated, giving a total of 60 sec of recorded data. In these experiments, the rubber seal (boot) that seals the grease in the CV joint housing was not installed for easy accessibility and visualization. Note that all tests were conducted at the position when the trunnion with the tri-axial force sensor is in the top position.

The force components inside the CV joint as measured with the tri-axial force transducer (Fx, Fy and Fz) show some variation with the CV joint stroke. Fx is the normal force P in calculating the friction coefficient, and shows fluctuation according to the direction of stroke motion. The Fy force shown in Figure 6(e), which is the main source of friction, is fluctuating with an amplitude of about 200 N at β=15°. Interestingly, the force Fz shown in Figure 6(f), which acts perpendicular to the CV joint

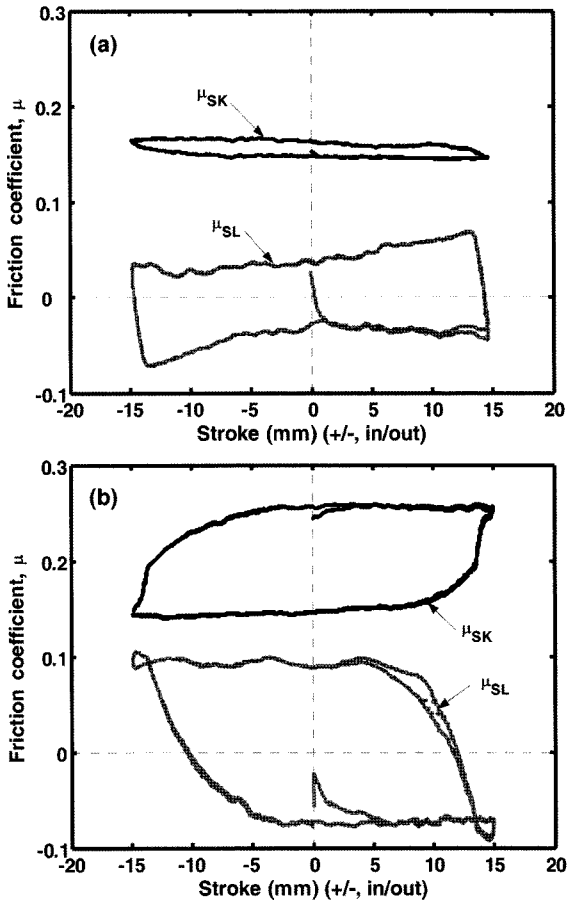

Figure 7. Combined friction coefficient μ, and the individual sliding resistance coefficient μ_{SL}: (a) at $\beta = 0°$; (b) at $\beta = 15°$.

shaft is negative during the inward stroke, which means that the force is acting downwards, or in compression in regards to the spider assembly, while Fz is positive during the outward stroke. The reason for this is because the contact between the roller and the housing does not occur at the center of the roller, thus giving rise to a net contact force in the z-direction. Substituting these measured forces in equation (1) (since the transducer is in top position in this case), the friction coefficient μ is plotted in Figure 6(h). The external thrust forces acting in the horizontal axial direction are shown in Figure 6(c). The trends follow the trends of the Fy force, which is the main force that affects the external friction force. However, this is the total force due to the forces from all three trunnions in the CV joint, whereas the internal trunnion forces were measured on only one of the trunnions. The value of the external thrust force is not of the same order as three times the internal friction force Fy due to the complicated CV joint kinematics. This clearly shows the inadequacy of the external thrust force, or GAF to accurately measure the internal friction in a CV joint. As

shown in Figure 6(b), slight torque changes during the experiment are attributed to small irregularities in the housing surface, with the changes being coincidental with the stroke changes.

The obtained friction coefficient versus stroke is plotted in Figure 7 for the two cases of extreme articulation angles (0° and 15°) under 160 Nm static torque. It is observed that the size of the hysteretic loops as well as the absolute mean value of the resultant friction coefficient increases with the increased articulation angle of 15°. Moreover, the obtained friction loops show that the inward stroke friction coefficient is more dependent on the articulation angle compared to the outward stroke friction. However, both friction loops in Figure 7(a) and Figure 7(b) never reach negative values during motion reversals. This seems counterintuitive as the friction coefficient is always positive even when motion is reversed. This is due to the fact that initial static friction exists during the torque loading, even before the stroking motion. The individual sliding resistance coefficient μ_{SL} also shows an increment of the loop amplitude comparing 0° to 15° with their mean value being about zero, Unlike the total friction coefficient that was always positive, μ_{SL} is positive during the roller up motion and negative during the down motion.

4.2. Parametric Investigation

After typical experiments were conducted, more detailed experiments were conducted to evaluate the effect of articulation angle, β, applied static torque, plunging velocity, and the rotational phase angle, φ, on the friction coefficient. Using the same test procedure described above, the magnitude of the friction coefficient loop for different articulation angles β under 160 Nm torque were extracted and plotted in Figure 8. Error bars represent the magnitude of the friction loop and the solid square symbols represent the average value of the loop. The results clearly show that both the amplitude of the friction loop and the average value of the friction coefficient increase with increasing articulation angle. Also, the increment is linear as seen by the dotted line of linear curve-fit in Figure 8.

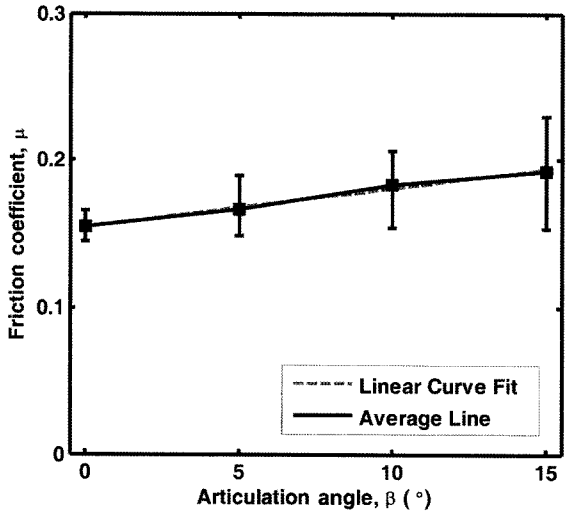

Figure 8. Changes of friction coefficient in terms of CV joint articulation angle β.

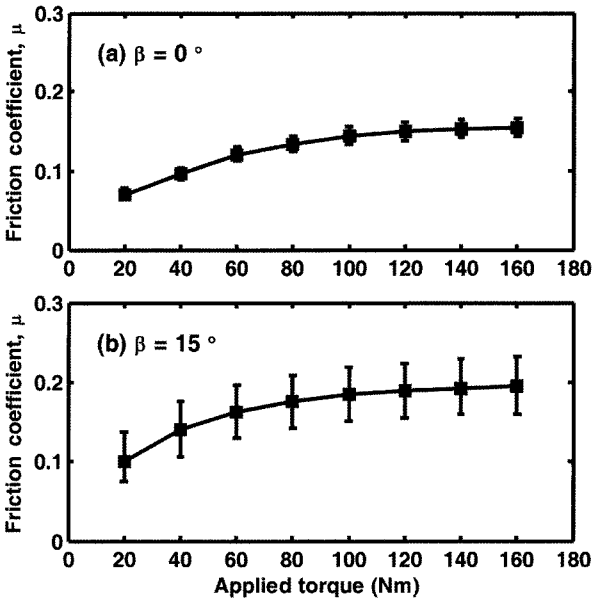

Figure 9. Dependency of the friction coefficient on applied torque: (a) $\beta = 0°$; (b) $\beta = 15°$.

Figure 9 summarizes the test results in terms of applied torque at the two extreme cases of articulation angles (0° and 15°), where the torque was varied from 20 Nm to 160 Nm. One readily observes that the fluctuation and average friction coefficient reach steady state values after 160 Nm torque. Thus, one could expect that the experimental results above 160 Nm will be similar to the actual values under the maximum engine torque (maximum CV joint torque is expected to be about 900 Nm for typical mid-size passenger cars).

Figure 10 shows the friction coefficient changes as a function of plunging velocities at 160 Nm of applied torque. The effect of the plunging velocity for the fixed stroke of +/−15 mm was investigated by changing the velocity from 1 mm/sec to 10 mm/sec for one cycle of stroking. As shown in the graphs in Figure 10, the trends of friction coefficient are almost identical for all velocity cases with the average value of about 0.15 and the loop amplitude of about 0.05. As the velocities are different, only the elapsed time of each test is different. This is due to the fact that the main contact is rolling, thus the "Stribeck" effect (friction values increase with increasing sliding velocity) is negligible even under boundary lubri-

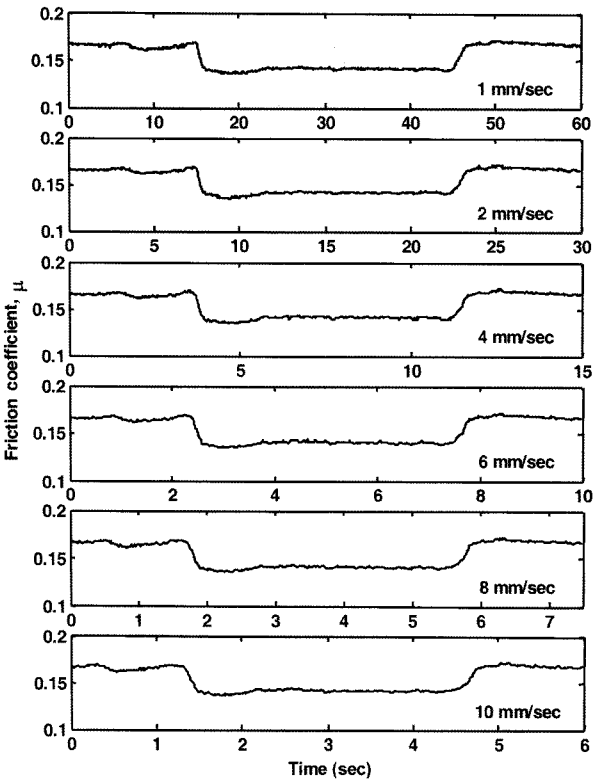

Figure 10. Friction coefficient trajectory under different plunging velocity.

cated conditions as is the case with CV joint greases.

These friction coefficient changes in terms of plunging velocity are summarized in Figure 11 at two extreme

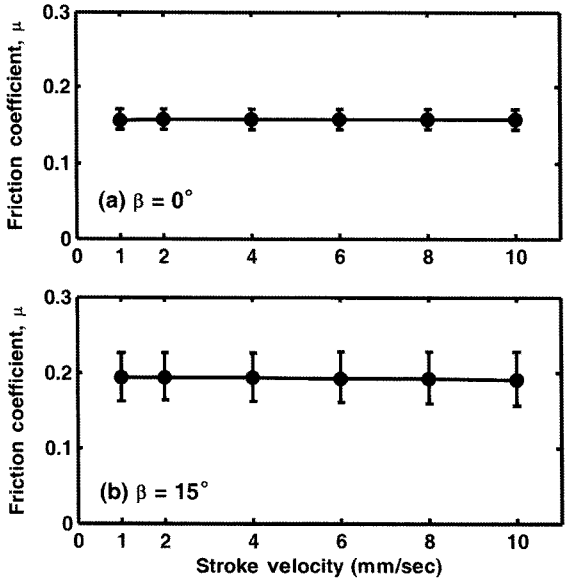

Figure 11. Dependency of the friction coefficient on plunging velocity: (a) $\beta = 0°$; (b) $\beta = 15°$.

articulation angles (0° and 15°) and 160 Nm torque. As shown in the results, the mean friction value and friction loop amplitude are almost consistent and independent of the plunging velocity. Thus, it is reasonable to assume that the friction properties at higher plunging velocities (estimated to be about 492 mm/sec under maximum engine rpm for typical mid-size passenger cars) will be similar to the values obtained under the present test conditions.

Rotational phase angle φ effects on the CV joint internal friction were investigated as the actual CV joint is rotating while driving. Tests were conducted at 26 equally spaced locations (phase angles) in the 360° of overall phase angles. Figure 12 shows the summary of the test results for the articulation angle of 0° and 15°, respectively, by plotting only the resultant friction coefficient and the amplitude of the friction coefficient loops. Again, the error bars represent the fluctuation amplitude of the friction coefficient during a cycle of CV joint stroking motion, and the solid circles the mean value at a phase angle.

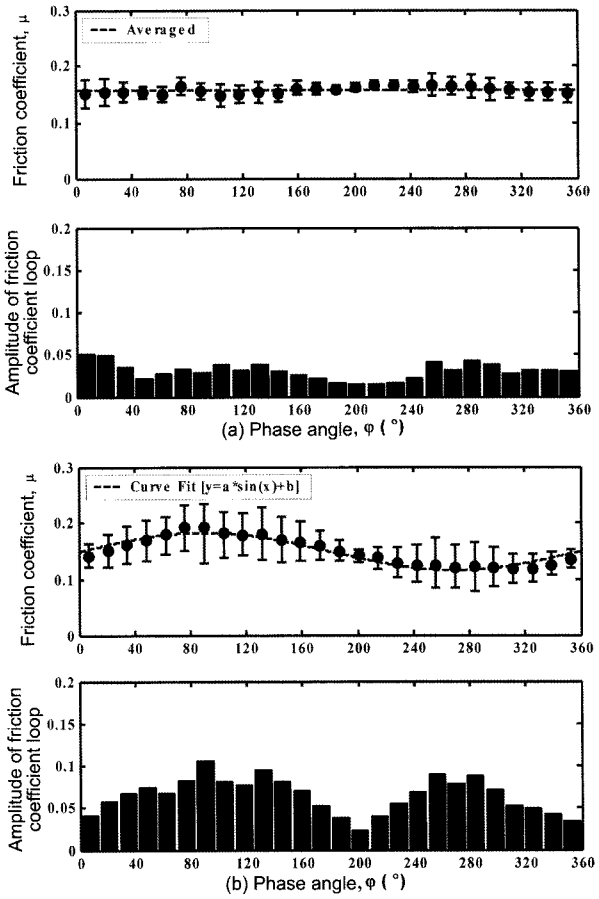

Figure 12. Friction coefficient and amplitude of friction coefficient loop in terms of the rotation phase angles: (a) $\beta = 0°$; (b) $\beta = 15°$.

The results clearly show that the friction coefficient changes in terms of the rotational phase angle due to the CV joint kinematics and orbiting trajectory of its center position. As clearly seen in Figure 12(a), the trend of the friction coefficient is constant, and the mean value of the friction coefficient is approximately 0.15. The amplitude of the friction coefficient loop (shown in the second plot of Figure 12(a)) is also nearly constant and less than 0.05 compared to the results for the case of β=15°, depicted in Figure 12(b). As expected, the articulation angle is the main source of generating the sinusoidal changes on the friction coefficient at a trunnion. However, the combined average friction coefficient at β=15° is almost the same as the averaged friction coefficient at β=0° with a value of 0.15. Thus, even though the amplitude of the friction coefficient loop is dependent on both the articulation and rotational phase angles, the average value of the friction coefficient loop is an inherent property and consistent at any position of the rotational phase angle and the articulation angle. As shown in Figure 12(b), the friction coefficient mean values, represented by the solid circles show a sinusoidal trend with phase angle changes, and one can thus use a simple sinusoidal function to curve-fit and describe this behavior. The amplitude of friction coefficient loop is plotted separately as shown in the bar graph in Figure 12(b). From this graph, we see that the friction coefficient amplitude of the loop is highest when the spider (that includes the tri-axial force transducer) is at 90° and 270°, i.e. when the force sensor is at top and bottom positions.

5. CONCLUSION

A CV joint friction apparatus was designed and constructed to perform realistic CV joint tests and measure internal CV joint forces including friction. This was accomplished using a tri-axial force transducer that was attached inside the CV joint and able to directly measure the internal forces in three orthogonal axes during dynamic CV joint motions, which has been impossible with the conventional test methods. The designed CV joint apparatus is fully under computer control and can perform versatile tests under realistic experimental conditions. By introducing a coordinate transformation matrix, the CV joint internal friction at any angle position was able to be globally evaluated. The experiments showed that the apparatus simulates actual CV joint movements and differences can readily be observed under different experimental conditions.

Specifically, parametric studies were also performed under different experimental conditions including the articulation angle, applied torque, plunging velocity and rotational phase angle. It was found that (i) larger articulation angle exhibits higher internal averaged friction coefficient and larger friction coefficient loop; (ii) the fluctuation loop and averaged friction coefficient reach steady state values after about 100 Nm applied torque; (iii) the averaged friction coefficient and fluctuation amplitude was constant and independent of the plunging velocity; and (iv) the averaged friction coefficient is almost independent of both articulation and rotational phase angles, although the amplitude of the loop is dependent on both parameters. The results clearly show that the internal friction measurement inside a CV joint is indispensable to evaluate the friction performance correctly without distortions due to the boot resistance, internal pressure, and other transmittance errors at the all connection parts.

ACKNOWLEDGEMENT–The author would like to express appreciation to Delphi Saginaw Steering Systems for useful advice in the design of CV joint friction apparatus.

REFERENCES

Bierman, J. (1999). Measurement system for CV joint efficiency. *SAE Paper No.*1999-01-0936, 203-209.

Gao, H., Barber, G. C. and Chu, H. (2002). Friction characteristics of a paper-based friction material. *Int. J. Automotive Technology* **3**, **4**, 171–176.

Jia, X., Jin, D., Ji, L. and Zhang, J. (2002). Investigation on the dynamic performance of the tripod-ball sliding joint with clearance in a clank-slider mechanism, Part1, Theoretical and experimental results. *J. Sound and Vibration* **252**, **5**, 919–933.

Kernizan, C., Jacobs, R. P. and Whitticar, D. J. (2002). Development of a constant velocity joint, CVJ, test stand to assess the performance of a series of greases. *NLGI Spokesman* **66**, **4**, 26–32.

Kochersberger, K. B. (2002). *Apparatus for Testing a Constant Velocity Joint and a Method Thereof.* United States Patent, 6,378,374 B2.

Philpott, M. L., Welcher, B. P., Pankow, D. R. and Vandenberg, D. (1996). Two phase circular regression algorithm for quantifying wear in CV joint ball race tracks. *Wear* **199**, **2**, 160–168.

Schmelz, F., Seherr-Thoss, C. H.-C. and Aucktor, E. (1992). *Universal Joints and Driveshafts: Dnalysis, Design, Applications (Translated by S.J. Hill and J.A. Tipper).* Springer-Verlag. New York.

Wagner, E. R. (1979). *Universal Joint and Driveshaft Design Manual: Advances in Engineering*, Series No. 7. Society of Automotive Engineers, Inc.. Warrendale. PA.